AMERICAN SOCIETY FOR MICROBIOLOGY | Journal of Virology®

VIRUS-CELL INTERACTIONS

Potato Spindle Tuber Viroid Modulates Its Replication through a Direct Interaction with a Splicing Regulator

Jian Jiang,[a] Heather N. Smith,[a] Di Ren,[a] Shachinthaka D. Dissanayaka Mudiyanselage,[a] Angus L. Dawe,[a] Lei Wang,[b,c] Ying Wang[a]

[a]Department of Biological Sciences, Mississippi State University, Mississippi State, Mississippi, USA
[b]Key Laboratory of Plant Molecular Physiology, CAS Center for Excellence in Molecular Plant Sciences, Institute of Botany, Chinese Academy of Sciences, Beijing, China
[c]University of Chinese Academy of Sciences, Beijing, China

ABSTRACT Viroids are circular noncoding RNAs (ncRNAs) that infect plants. Despite differences in the genetic makeup and biogenesis, viroids and various long ncRNAs all rely on RNA structure-based interactions with cellular factors for function. Viroids replicating in the nucleus utilize DNA-dependent RNA polymerase II for transcription, a process that involves a unique splicing form of transcription factor IIIA (TFIIIA-7ZF). Here, we provide evidence showing that potato spindle tuber viroid (PSTVd) interacts with a TFIIIA splicing regulator (ribosomal protein L5 [RPL5]) *in vitro* and *in vivo*. PSTVd infection compromises the regulatory role of RPL5 over splicing of *TFIIIA* transcripts, while ectopic expression of RPL5 reduces TFIIIA-7ZF expression and attenuates PSTVd accumulation. Furthermore, we illustrate that the RPL5 binding site on the PSTVd genome resides in the central conserved region critical for replication. Together, our data suggest that viroids can regulate their own replication and modulate specific regulatory factors leading to splicing changes in only one or a few genes. This study also has implications for understanding the functional mechanisms of ncRNAs and elucidating the global splicing changes in various host-pathogen interactions.

IMPORTANCE Viroids are the smallest replicons among all living entities. As circular noncoding RNAs, viroids can replicate and spread in plants, often resulting in disease symptoms. Potato spindle tuber viroid (PSTVd), the type species of nuclear-replicating viroids, requires a unique splicing form of transcription factor IIIA (TFIIIA-7ZF) for its propagation. Here, we provide evidence showing that PSTVd directly interacts with a splicing regulator, RPL5, to favor the expression of TFIIIA-7ZF, thereby promoting viroid replication. This finding provides new insights to better understand viroid biology and sheds light on the noncoding RNA-based regulation of splicing. Our discovery also establishes RPL5 as a novel negative factor regulating viroid replication in the nucleus and highlights a potential means for viroid control.

KEYWORDS Viroid, noncoding RNA, alternative splicing, host-viroid interactions

Viroids are circular noncoding RNAs (ncRNAs) that infect plants, often leading to disease symptoms (1). This group of organisms are by far the smallest replicons among all biological entities on Earth (2, 3). Five structural domains are defined in the RNA genome of viroids in the family *Pospiviroidae*: the left terminal domain, the pathogenicity domain, the central domain, the variable domain, and the right terminal domain (4–7). The type species in the *Pospiviroidae* is the potato spindle tuber viroid (PSTVd). The PSTVd genome comprises 27 RNA loop motifs flanked by short double helices. These loop motifs are designated numerically in order from the left terminal

Received 8 June 2018 **Accepted** 29 July 2018
Accepted manuscript posted online 1 August 2018
Citation Jiang J, Smith HN, Ren D, Dissanayaka Mudiyanselage SD, Dawe AL, Wang L, Wang Y. 2018. Potato spindle tuber viroid modulates its replication through a direct interaction with a splicing regulator. J Virol 92:e01004-18. https://doi.org/10.1128/JVI.01004-18.
Editor Anne E. Simon, University of Maryland, College Park

Address correspondence to Ying Wang, wang@biology.msstate.edu.
This article is dedicated to the late Biao Ding.

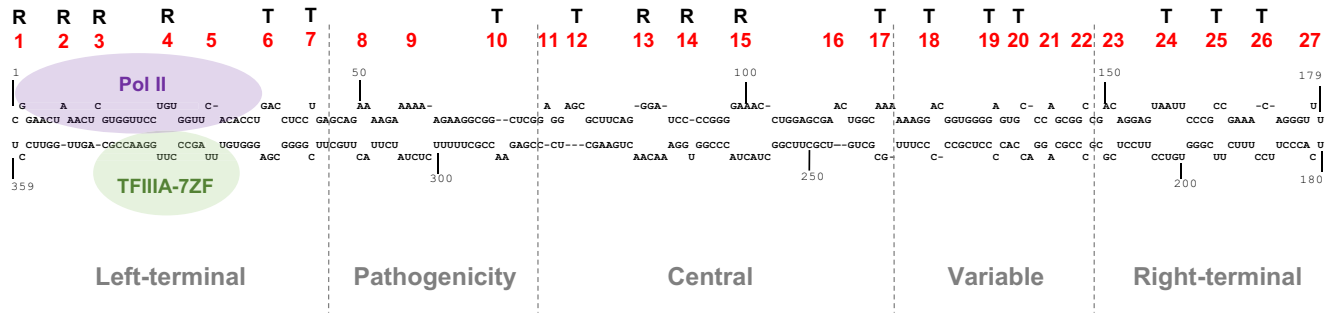

FIG 1 PSTVd secondary structure and the binding sites of Pol II and TFIIIA-7ZF (5–7). The proposed secondary structure of PSTVd^{Int} (the intermediate strain) genome is shown, with all the loops labeled numerically in red. "R" denotes the function of an RNA motif controlling PSTVd replication; "T" denotes the function of an RNA motif controlling PSTVd systemic trafficking. The limits of the five domains are defined by the dashed lines.

loop (loop 1) to the right terminal loop (loop 27). Loops 1 to 4 and loops 13 to 15 have been shown to be critical for replication (Fig. 1) (8–13).

Despite having the simplest genetic makeup, the mechanisms behind how viroids coopt cellular factors to effectively propagate themselves remain elusive (2, 14, 15). PSTVd, and other viroids in the *Pospiviroidae*, employ DNA-dependent RNA polymerase II (Pol II) for RNA-templated transcription (16–18). A specific splicing form of transcription factor IIIA containing seven zinc finger domains (ZFs), termed TFIIIA-7ZF, is required to facilitate Pol II-dependent transcription of the PSTVd template (19). The binding sites for Pol II and TFIIIA-7ZF have both been mapped *in vitro* to PSTVd left terminal domain (Fig. 1) (13, 19). A previous study showed that plant ribosomal protein L5 (RPL5) regulates alternative splicing (AS) of *TFIIIA* transcripts by binding to a conserved 5S rRNA-mimic structure that resides in an intron in the pre-mRNA (termed AS intron here) (20). RPL5 binding favors removal of the AS intron, resulting in the production of the full-length protein (containing nine ZFs; termed TFIIIA-9ZF) and the reduced accumulation of TFIIIA-7ZF (20). Interestingly, the physical interaction between RPL5 (cloned from a non-host plant, *Arabidopsis thaliana*) and PSTVd is supported by an *in vitro* assay (21), suggesting a possibility that PSTVd interacts with RPL5 to manipulate AS of *TFIIIA* for optimized replication.

Here, we experimentally tested this possibility and found that modulating the expression of RPL5 indeed impacts PSTVd replication through regulating the expression of TFIIIA-7ZF. In addition, we found that the RPL5 binding site resides in the PSTVd central conserved region (CCR), which is within the central domain and is conserved in members of the genus *Pospiviroid* (5, 7). Taken together, our data shed light on how PSTVd modulates the host machinery to favor its replication and also on how noncoding RNAs regulate alternative splicing of cellular transcripts.

RESULTS

RPL5 interacts with PSTVd. RPL5 cloned from *A. thaliana* has been shown to interact with PSTVd in an electrophoretic mobility shift assay (EMSA) (21). Here, we first confirmed that RPL5 cloned from a host plant, *Nicotiana benthamiana*, also interacts with PSTVd. As shown in Fig. 2, the interaction between NbRPL5 and PSTVd was inferred by the formation of several high molecular weight complexes in EMSA, and the corresponding dissociation constant (K_d) was estimated (0.214 μM) based on three biological replicates. This value resembles the K_d reported for the AtRPL5-PSTVd interaction (21). To fully understand the biology of this interaction, we sought to compare the binding affinity of RPL5 with 5S rRNA, the AS intron and PSTVd. Based on the EMSA results, RPL5 exhibited a weaker affinity with 5S rRNA (K_d = 2.92 μM) and the weakest affinity with the AS intron (K_d = 9.9 μM) (Fig. 2). These data are comparable with the reported affinity of AtRPL5 with the corresponding RNA substrates (20, 22). Moreover, the observation that NbRPL5 has the strongest affinity for binding with PSTVd provides a biochemical basis for PSTVd competition of RPL5 for function.

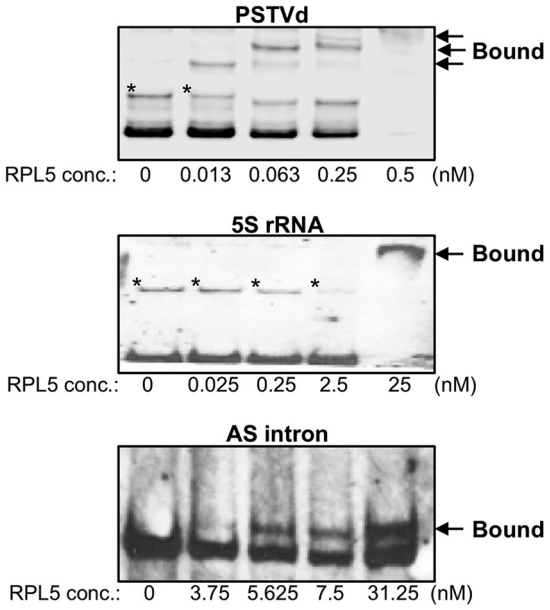

FIG 2 EMSA results showing RPL5 bound to PSTVd, 5S rRNA, and the AS intron (panels from top to bottom, respectively). The RPL5 concentration for each reaction was listed. An "*" denotes the unbound probes showing a distinct mobility on the gel, likely due to the formation of alternative structures.

We then performed RNA immunoprecipitation (RIP), followed by next-generation sequencing, to test the *in vivo* interaction between NbRPL5 and PSTVd. As shown in Fig. 3, we successfully immunoprecipitated the endogenous NbRPL5 protein from PSTVd-infected plants. After three biological repeats of immunoprecipitation, we then constructed deep-sequencing libraries using the RNAs purified from the input lysate and the immunoprecipitate (IP) fraction for each replicate. After sequencing, the processed reads were mapped to the full-length cDNA sequences of PSTVd and 5S rRNA using local BLAST tools. 5S rRNA served as a positive control based on its binding with RPL5 for ribosomal subunit formation *in vivo* (23). The reads mapped to 5S rRNA were generally present in 50- to 100-fold larger amounts than those mapped to PSTVd in each library, reflecting that 5S rRNA is much more abundant than PSTVd in plants. After normalization to the corresponding input, a similar

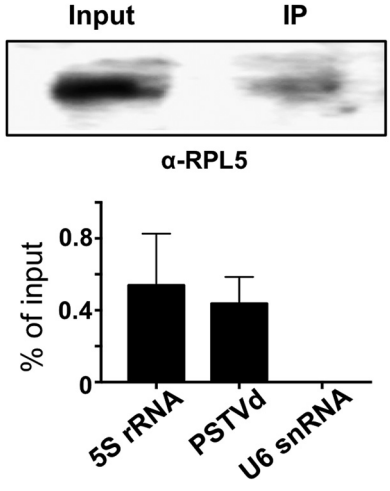

FIG 3 RNA-immunoprecipitation-Seq. The top panel shows a representative immuno-blotting result of RPL5 in input lysate and IP fraction. The bottom panel shows the fraction (%) of IP RNAs normalized to the corresponding input samples.

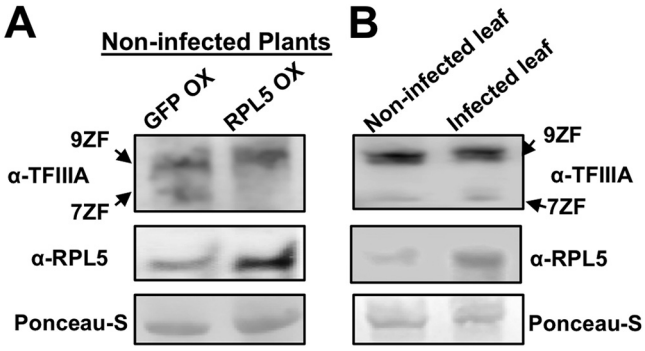

C

	Mock			PSTVd-infected			Ratio	FDR
	1	2	3	1	2	3		
TFIIIA-9ZF	19.71	8.70	6.00	7.83	7.57	0.00	0.45	0.627
TFIIIA-7ZF	35.84	54.31	35.07	52.26	52.62	58.61	1.31	0.569
RPL5	166.63	153.29	147.97	350.8	317.72	289.99	2.05	0.003

FIG 4 PSTVd infection compromises RPL5 function. (A) Immunoblotting results show the expression of RPL5, TFIIIA-7ZF, and TFIIIA-9ZF in noninfected leaves following GFP overexpression (OX) or RPL5 OX. (B) Immunoblotting results showing the expression of RPL5, TFIIIA-7ZF, and TFIIIA-9ZF in noninfected and PSTVd-infected leaves. (C) In PSTVd-infected tomato leaves, *RPL5* transcripts were significantly upregulated, *TFIIIA-9ZF* was slightly repressed, while *TFIIIA-7ZF* was slightly elevated. 9ZF and 7ZF refer to TFIIIA-9ZF and TFIIIA-7ZF, respectively. FDR, adjusted *P* value based on the whole RNA-Seq data.

enrichment for PSTVd and 5S rRNA was observed in the IP (Fig. 3). U6 snRNA served as a known negative control (19), and we accordingly did not find U6 snRNA reads in the IP fraction in any of the biological repeats, despite their presence in all three input libraries (Fig. 3). Thus, our data support the specific RPL5-PSTVd interaction in plants.

PSTVd infection induces RPL5 but also affects RPL5-based regulation over TFIIIA splicing. Using a reporter system, a previous study has shown that overexpression of RPL5 leads to removal of the AS intron, thus suppressing the expression of *TFIIIA-7ZF* (20). Here, we first overexpressed NbRPL5 in noninfected *N. benthamiana* plants using agroinfiltration and then examined the accumulation of TFIIIA protein variants using immunoblotting. Previously, we developed a polyclonal rabbit antiserum that specifically recognized both TFIIIA-7ZF and TFIIIA-9ZF proteins (19), facilitating detection of both proteins on the same blot. As shown in Fig. 4A, we confirmed that overexpression of RPL5 indeed significantly suppressed the expression of TFIIIA-7ZF protein in noninfected plants.

To test whether PSTVd affects the regulatory role of RPL5 over TFIIIA splicing in infected plants, we performed immunoblotting to compare the endogenous accumulation of RPL5 and two forms of TFIIIA proteins in noninfected and PSTVd-infected leaves at the same developmental stage. The expression of TFIIIA-9ZF was largely unaffected, while TFIIIA-7ZF remained the same or slightly elevated in PSTVd-infected plants. Meanwhile, we observed an increase in the accumulation of RPL5 protein (Fig. 4B). This is largely in agreement with a recent transcriptome sequencing (RNA-Seq) data set of PSTVd-infected tomato leaves. By reanalyzing this published data set, we observed a slight reduction of *SlTFIIIA-9ZF* and a slight increase of *SlTFIIIA-7ZF* (both from the Solyc06g007660 locus), as well as a 2-fold increase in *SlRPL5* (Solyc06g007670.2.1) (24) (Fig. 4C). Although the change in *SlRPL5* expression is significant based on the statistical analysis indicated by the value of the false discovery rate (FDR), neither SlTFIIIA-7ZF nor SlTFIIIA-9ZF showed significant changes (Fig. 4C). Interestingly, the upregulation of RPL5 was not associated with a significant downregulation of TFIIIA-7ZF in PSTVd-infected plants, which is in contrast to the effects of RPL5 overexpression in noninfected plants (Fig. 4A). This observation supports that PSTVd compromises the regulatory role of RPL5 over *TFIIIA* splicing. Despite

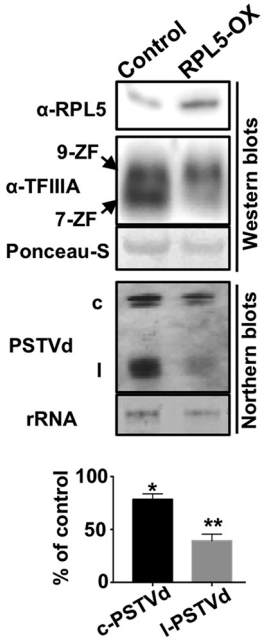

FIG 5 Ectopic expression of RPL5 represses PSTVd replication. Blotting results show that overexpression of RPL5 in infected plants reduced the accumulation of PSTVd, which correlated with the reduction of TFIIIA-7ZF. 9ZF and 7ZF refer to TFIIIA-9ZF and TFIIIA-7ZF, respectively. "c" and "l" indicate the circular and linear PSTVds, respectively. Student *t* tests were performed to calculate the significant changes of PSTVd (*, $P < 0.05$; **, $P < 0.01$).

the induction of RPL5 in PSTVd-infected plants, some portion of RPL5 may not be available for splicing regulation, possibly attributable to the PSTVd occupancy through the direct RPL5-PSTVd interaction.

Ectopic expression of RPL5 in infected plants attenuates PSTVd replication. If the RPL5-PSTVd interaction indeed interferes the RPL5 regulation over splicing of *TFIIIA*, further elevation of RPL5 in PSTVd-infected plants should lead to the reduction of TFIIIA-7ZF, which would result in reduced PSTVd titer. To this end, we ectopically overexpressed NbRPL5 in PSTVd-infected plants using agroinfiltration and examined the PSTVd titer in the nucleus. All test plants were first subjected to Northern blotting before agroinfiltration to ensure that they contained similar PSTVd titers in total leaf extracts. In this assay, we found that overexpression of NbRPL5 in PSTVd-infected leaves indeed reduced the PSTVd titer (Fig. 5). It is striking that the linear PSTVd (likely the replication intermediate) displayed a 2-fold reduction compared to the control, which may suggest the effective inhibition of PSTVd replication (Fig. 5). This phenomenon correlated well with the reduction of NbTFIIIA-7ZF protein (Fig. 5). Therefore, our data supported that the interaction between PSTVd and RPL5 is critical for PSTVd replication, probably through regulating TFIIIA splicing.

RPL5 binds PSTVd loop E within the central conserved region. Based on the aforementioned findings, we further reasoned that the PSTVd RNA structure(s) recognized by RPL5 should be critical for PSTVd replication. This is because if the RPL5-PSTVd interaction is critical for modulating TFIIIA-7ZF expression, PSTVd variants lacking the capacity to manipulate the function of RPL5 may encounter an insufficient amount of TFIIIA-7ZF in host cells, thus leading to deficient propagation. In an EMSA, we chose three PSTVd loop mutants that abolish loops 4, 15, and 26, respectively. Loop 26 is critical for PSTVd systemic trafficking, while loops 4 and 15 (also termed loop E) are critical for PSTVd replication (Fig. 1) (8). The region harboring loops 1 to 4 is the binding site for TFIIIA-7ZF and Pol II (13, 19), and the region containing loop 26 is the binding site for NbTFIIIA-9ZF (19). However, specific host factor(s) interacting with the regions containing loops 13 to 15 (part of the CCR) remain unknown. The involvement in

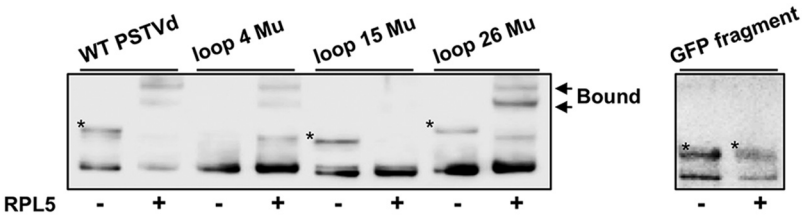

FIG 6 RPL5 binding to loop 15 in the central conserved region of PSTVd. Mutations abolishing either loop 4 or loop 26 did not affect PSTVd binding to RPL5 (0.3125 nM when supplied) compared to that of wild-type PSTVd. In contrast, mutations abolishing loop 15 strongly reduced the binding of PSTVd to RPL5. A *GFP* mRNA fragment (~300 nucleotides; corresponding to the C terminus) served as a negative control. "*" depicts the unbound probes that showed a distinct mobility on the gel, likely due to the formation of alternative structures. The presence or absence of RPL5 protein in each reaction is indicated by "+" or "−" symbols, respectively.

replication or trafficking of the selected loop variants has been confirmed previously (8, 9, 25). As shown in Fig. 6, RPL5 showed comparable affinity to wild type and mutants with an abolished loop 4 or loop 26, but it showed a significant reduction in affinity to the mutant with abolished loop 15. In addition, to further ensure the binding specificity of RPL5, we included a *GFP* fragment (~300 nucleotides) as a negative control, which showed no binding with RPL5 under the same test condition (Fig. 6). Thus, the data are consistent with the notion that RPL5 binds to a PSTVd region critical for replication, which further supports the functional importance of the RPL5-PSTVd interaction.

DISCUSSION

TFIIIA and RPL5 have long been speculated to be host factors for PSTVd (26). Until recently, emerging evidence supported the function of a TFIIIA splicing variant, TFIIIA-7ZF, in facilitating Pol II-dependent transcription of PSTVd RNA genome (19). Our data presented here confirmed that RPL5 is a novel host factor for PSTVd infection. We also illustrated that RPL5 binds to a PSTVd region within the CCR for function. RPL5-based regulation of *TFIIIA* splicing is conserved in land plants (20, 27), while the CCR in PSTVd is conserved in the genus *Pospiviroid* (4, 5). Therefore, the RPL5-PSTVd interaction has the potential to exist in a broad spectrum of host-viroid interactions. With the discovery of this functional interaction, we also provided mechanistic insights to better understand the cellular machinery coopted by PSTVd for propagation. The cluster of loop motifs at the left terminal domain interacts with TFIIIA-7ZF and Pol II (13, 19) to initiate transcription, while the CCR, containing the loop E motif, interacts with RPL5 to modulate the expression of TFIIIA-7ZF. It is noteworthy that PSTVd loop E motif is critical for replication, host range, tissue tropism, and symptoms (9, 10, 12, 25, 28–30). Thus, it is worth testing whether the RPL5-PSTVd interaction also mediates the functional versatility of PSTVd loop E.

It has been well documented that PSTVd infection, like other pathogens, globally alters host gene expression (24, 31, 32). Furthermore, emerging evidence supports that PSTVd infection globally alters the AS of host transcripts as well, suggesting that PSTVd interferes with the host AS to modulate plant gene expression at the posttranscriptional level (24). Similar phenomena have also been observed during the infection of viruses and oomycetes (33–35). Noteworthy is that several specific splicing variants have been shown to play critical roles in host-microbe interactions (19, 36, 37), although how microbes achieve such regulation remains elusive. One possibility is that PSTVd interacts with one or a few master regulator(s) to impair the global AS of plant transcripts. In line with this possibility, there is one plant endogenous lncRNA that employs such a mechanism to regulate splicing of a group of gene transcripts (38). While this hypothesis for explaining viroid-induced AS changes is still worth testing, our finding shows that PSTVd can coopt specific AS regulator(s), such as RPL5, to directly affect one or a few genes, clearly reflecting the complexity underlying the interplay between PSTVd and the host AS machinery. Given the observation that some viruses

and oomycetes also interfere with the host AS machinery, our finding has profound implications in understanding plant-pathogen interactions.

Lastly, modulating RPL5 expression may be a novel strategy to combat viroid diseases. To date, most of the efforts have been focused on (i) exploiting RNA silencing principles, (ii) screening resistant plant cultivars, (iii) generating transgenic plants expressing a double-stranded RNA-specific RNase, and (iv) preinfection with mild-symptom strains to control viroid disease (39–41). We show here that the overexpression of RPL5 can effectively restrain replication of PSTVd in infected leaves (Fig. 5), supporting RPL5 as a bona fide negative regulator of viroid replication that could be exploited in future breeding efforts.

MATERIALS AND METHODS

Plant growth. *N. benthamiana* plants were grown in a growth chamber at 25°C and with a 16/8-h light/dark cycle. Seedlings with four true leaves were inoculated with water or water containing 150 ng of PSTVd^{Int} (the intermediate strain) RNA. After 3 weeks postinoculation, the leaf samples were collected and the PSTVd infection was verified by Northern blotting, as described previously (19). Agroinfiltration followed an established protocol described previously in detail (19).

Cloning. RPL5 cDNA from *N. benthamiana* plants was cloned using primers (forward, 5′-CACCATG GCCTTCATCAAAGTCCAG-3′; reverse, 5′-TTACTCGTCATCCTCATCATCATCG-3′) for pENTR/D/TOPO cloning (Thermo Fisher Scientific, Waltham, MA). Using LR clonase II (Thermo Fisher Scientific), pENTR-NbRPL5 was recloned into pDEST17 vector (Thermo Fisher Scientific) for protein expression in bacteria, and into pEARLEYGATE201 vector (from ABRC) for protein expression in plants. The AS intron was cloned using primers (forward, 5′-TGCAAGAGAGGCCATTTGCATGCC-3′; reverse, 5′-TGCAAGAGATGTCTCGTCAAGTG-3′) and *N. benthamiana* genomic DNA. The PCR product was inserted into pCR4 vector according to the manufacturer's manual (Thermo Fisher Scientific). The GFP300 fragment was cloned using pH7GW2 vector as a template and primers (forward, 5′-GGAGTACAACTACAACAGCCAC-3′; reverse, 5′-TTACTTGT ACAGCTCGTCCATGCCG-3′). The PCR product was inserted into pGEMT (Promega, Madison, WI). All the constructs were verified by sanger sequencing. Other DNA constructs for generating EMSA substrates, pDONR221-T3-PSTVd and pGEMT-5SrRNA, have previously been reported (19).

To generate the RNA substrates for EMSA, pCR4-AS-Intron was linearized using NotI (New England BioLabs, Ipswich, MA) and was subject to *in vitro* transcription using a T3 Megascript kit (Thermo Fisher Scientific). pDONR221-T3-PSTVd was linearized using SmaI (New England BioLabs) and was subject to *in vitro* transcription using a T3 Megascript kit (Thermo Fisher Scientific). pGEMT-5SrRNA was linearized using NdeI (New England BioLabs) and was subject to *in vitro* transcription using a T7 Megascript kit (Thermo Fisher Scientific). pGEMT-GFP300 was linearized using NcoI (New England BioLabs) and was subject to *in vitro* transcription using a SP6 Megascript kit (Thermo Fisher Scientific). Loop 4 and loop 26 mutants are loop-close mutants described in Zhong et al. (8), and the loop 15 mutant is also a loop-close mutant generated via a site-directed mutagenesis using primer pairs (forward, 5′-CCTCACTAAAGGGTA ATAGCTGGAGC-3′; reverse, 5′-CAGTTCGCTCCAGCTATTACCTA-3′) and the wild-type pDONR221-T3-PSTVd template, changing 95-GGGGAAAC-102 to 95-GGGTAATAG-103. All plasmids containing the mutant cDNAs were linearized using SmaI and were subject to *in vitro* transcription using a T3 Megascript kit (Thermo Fisher Scientific).

Ribosomal protein L5 purification. Recombinant RPL5 protein with a 6× histidine tag was expressed in *Escherichia coli* Rosetta strain (EMD Millipore, Burlington, MA). Cells were grown overnight at 37°C in Luria-Bertani (LB) medium supplied with ampicillin (0.1 mg/ml) and chloramphenicol (0.034 mg/ml). An aliquot of cells with an optical density at 600 nm (OD_{600}) of 0.1 was inoculated into fresh LB medium supplied with antibiotics the next day. Once the cell density (i.e., the OD_{600}) reached 0.5 to 0.7, 0.4 mM IPTG (isopropyl-β-D-thiogalactopyranoside; final concentration) was added to the culture to induce protein expression. After inducing for 16 h at room temperature, 250 ml of culture was harvested by centrifugation at 8,000 rpm for 8 min. Pellets were resuspended in a lysis buffer containing 50 mM NaH_2PO_4, 300 mM NaCl (pH 8.0), and 20 mM phenylmethylsulfonyl fluoride and sonicated to lyse the cells. Homogeneous cell lysate was then centrifuged at 10,800 rpm for 30 min at 4°C. The supernatant was collected and incubated for 1 h with 4 ml of 50% slurry of Ni FF resin (New England BioLabs) before being loading onto an empty EconoPac gravity-flow column (Bio-Rad Laboratories, Hercules, CA). The resin was then washed eight times with washing buffer (50 mM NaH_2PO_4, 300 mM NaCl, 100 mM imidazole). The protein was then released with elution buffer (50 mM NaH_2PO_4, 300 mM NaCl, 400 mM imidazole) and concentrated using an Amicon protein concentrator (MilliporeSigma). Proteins were then separated by SDS–10% PAGE electrophoresis, followed by Coomassie blue staining and destaining to estimate the concentration using a bovine serum albumin standard as reference.

EMSAs. Binding assays that contained RNA in the absence or presence of different amounts of RPL5 protein were incubated at 28°C for 30 min. Binding buffer for PSTVd and RPL5 was composed of 50 mM Tris-HCl (pH 7.5), 50 mM NaCl, 1 mM EDTA, 10 mM DTT, and 10% glycerol. Binding buffer for 5S rRNA/the AS intron and RPL5 consisted of 20 mM Tris-HCl (pH 7.5), 7 mM $MgCl_2$, 1 mM dithiothreitol, 70 mM KCl, and 10% glycerol. Electrophoresis for the binding assay was performed at 4°C in 8% polyacrylamide (29:1) gels at 150 V using 1× TAE (40 mM Tris, 20 mM acetate, and 1 mM EDTA [pH 8.6]), with 1 h for the AS intron and 5S rRNA or 1.6 h for PSTVd. The RNAs were then transferred to Hybond-XL nylon membranes (Amersham Biosciences, Little Chalfont, United Kingdom) by a Bio-Rad Laboratories semidry transfer cassette and immobilized by a UV-cross-linker (UVP, Upland, CA). The RNAs were then detected by

digoxigenin-labeled UTP probes. For PSTVd detection, probes were obtained by transcribing a HindIII-linearized pInt(−) template (25) using a T7 polymerase MAXIscript kit (Thermo Fisher Scientific). For detecting 5S rRNA, probes were transcribed from a NcoI-linearized pGEMT-5SrRNA template (19) using a SP6 MAXIscript kit (Thermo Fisher Scientific). For the AS intron detection, probes were generated by *in vitro* transcription of a SpeI-linearized pCR4-AS-intron template using a T7 MAXIscript kit. For detection of GFP300, probes were generated by *in vitro* transcription of a SpeI-linearized pGEMT-GFP300 template using a T7 MAXIscript kit. RNA shifting was determined either by film developer or a C-digit blot scanner (LI-COR Biosciences, Lincoln, NE). The intensity of each band on the membrane was quantified using ImageJ (https://imagej.nih.gov/ij/). The binding curves were obtained by plotting the fraction of RNA bound to proteins.

RNA immunoprecipitation and immunoblotting. RNA RIP was performed according to a previously described protocol (19). Briefly, plant leaves were harvest from PSTVd-infected leaves, and the resulting extracts were subject to nuclei enrichment and nuclear lysis (19). The lysate was incubated with anti-RPL5 (Aviva Systems Biology, San Diego, CA) and magnetic protein A/G beads (Thermo Fisher Scientific) according to the manufacturer's instructions. The input lysate and purified fractions were subject to immunoblotting and RNA library construction (after RNA purification).

For immunoblotting, we followed the previously described protocol (19). Polyclonal antibodies against TFIIIA were diluted at 1:800 (19), and the polyclonal anti-RPL5 antibodies (Aviva Systems Biology) were diluted at 1:2,000. Horseradish peroxidase-conjugated anti-rabbit serum (Bio-Rad) was diluted at 1:3,000.

RNA extraction and library preparation. RNAs were isolated using RNAzol (Molecular Research Center, Cincinnati, OH) and then subjected to the first-strand cDNA synthesis, followed by second-strand cDNA synthesis (New England BioLabs, Ipswich, MA). Fragmentase (New England BioLabs) was used to digest double-strand cDNA for 30 min at 37°C to obtain size fragment about 50 to 200 bp. The fragmented DNA was then purified using a DNA Clean and Concentrator apparatus (Zymo Research, Irvine, CA). Purified DNA from the previous step was then treated for end preparation and adaptor ligation using the NEBNext Ultra II Directional Library Prep Kit for Illumina (New England BioLabs). PCR was conducted subsequently to enrich the adaptor-ligated DNA. After collecting size-exclusive DNA using a AxyPrep PCR Mag Cleaning-Up kit (Thermo Fisher Scientific), the quality of the library was checked using a bioanalyzer (Agilent, Santa Clara, CA).

RNA-Seq data processing and mapping. Single-end RNA-Seq reads were processed using Trimmomatic Ver0.36 (42) to eliminate adaptors and low-quality reads, with a minimum length of 36 bp and a minimum threshold quality score of 25. A transcriptome was generated from transcripts of the *N. benthamiana* draft genome version 1.0.1 (43) using the available annotation as well as adding the sequences of $PSTVd^{Int}$ and the 5S rRNA. Reads were then mapped to the transcriptome using Bowtie (v2.3.4) (44) with the "very-sensitive" mode to obtain the total number of mapped reads. The mapped reads were then used in BLASTn-short (optimized for sequences shorter than 50 bp) to obtain reads mapping to the cDNA sequences of 5S rRNA, PSTVd, and U6 snRNA. The values of transcripts per million were calculated by dividing the number of reads mapped to each RNA by the total mapped reads. The bioinformatics methods for analyzing the published tomato RNA-Seq data have been described in detail by Zheng et al. (24). The reads mapped to *TFIIIA* and *RPL5* cDNA sequences were extracted to generate the Fig. 4C in this study.

Accession number(s). The RIP-Seq data have been deposited at NCBI SRA under accession number PRJNA473206. The tomato RNA-Seq data were deposited at NCBI SRA under accession number PRJNA353731.

ACKNOWLEDGMENTS

We express our gratitude for the technical support from Luis Fernando Rodriguez-Caro in our department. We are grateful for the support from Yi Zheng and Zhangjun Fei at Cornell University. We also thank the anonymous reviewers for their constructive suggestions.

This study was supported by grants from the U.S. National Science Foundation (IOS-1564366) and the Strategic Research Initiative at the College of Arts and Sciences, Mississippi State University, to Y.W. The authors declare that they have no conflict of interest.

Y.W. designed the research. J.J., H.N.S., S.D.D.M., and Y.W. performed the research. J.J., H.N.S., D.R., A.L.D., L.W., and Y.W. analyzed data. J.J., H.N.S., D.R., L.W., A.L.D., and Y.W. wrote the article.

REFERENCES

1. Katsarou K, Rao AL, Tsagris M, Kalantidis K. 2015. Infectious long non-coding RNAs. Biochimie 117:37–47. https://doi.org/10.1016/j.biochi.2015.05.005.
2. Ding B. 2009. The biology of viroid-host interactions. Annu Rev Phytopathol 47:105–131. https://doi.org/10.1146/annurev-phyto-080508-081927.
3. Flores R, Gago-Zachert S, Serra P, Sanjuan R, Elena SF. 2014. Viroids: survivors from the RNA world? Annu Rev Microbiol 68:395–414. https://doi.org/10.1146/annurev-micro-091313-103416.
4. Keese P, Symons RH. 1985. Domains in viroids: evidence of intermolecular RNA rearrangements and their contribution to viroid evolution. Proc

Natl Acad Sci U S A 82:4582–4586. https://doi.org/10.1073/pnas.82.14.4582.
5. Lopez-Carrasco A, Flores R. 2017. Dissecting the secondary structure of the circular RNA of a nuclear viroid in vivo: a "naked" rod-like conformation similar but not identical to that observed in vitro. RNA Biol 14:1046–1054. https://doi.org/10.1080/15476286.2016.1223005.
6. Gast FU, Kempe D, Spieker RL, Sanger HL. 1996. Secondary structure probing of potato spindle tuber viroid (PSTVd) and sequence comparison with other small pathogenic RNA replicons provides evidence for central noncanonical base-pairs, large A-rich loops, and a terminal branch. J Mol Biol 262:652–670. https://doi.org/10.1006/jmbi.1996.0543.
7. Giguere T, Adkar-Purushothama CR, Perreault JP. 2014. Comprehensive secondary structure elucidation of four genera of the family *Pospiviroidae*. PLoS One 9:e98655. https://doi.org/10.1371/journal.pone.0098655.
8. Zhong X, Archual AJ, Amin AA, Ding B. 2008. A genomic map of viroid RNA motifs critical for replication and systemic trafficking. Plant Cell 20:35–47. https://doi.org/10.1105/tpc.107.056606.
9. Zhong X, Leontis N, Qian S, Itaya A, Qi Y, Boris-Lawrie K, Ding B. 2006. Tertiary structural and functional analyses of a viroid RNA motif by isostericity matrix and mutagenesis reveal its essential role in replication. J Virol 80:8566–8581. https://doi.org/10.1128/JVI.00837-06.
10. Gas ME, Hernandez C, Flores R, Daros JA. 2007. Processing of nuclear viroids in vivo: an interplay between RNA conformations. PLoS Pathog 3:e182. https://doi.org/10.1371/journal.ppat.0030182.
11. Owens RA, Baumstark T. 2007. Structural differences within the loop E motif imply alternative mechanisms of viroid processing. RNA 13:824–834. https://doi.org/10.1261/rna.452307.
12. Baumstark T, Schroder AR, Riesner D. 1997. Viroid processing: switch from cleavage to ligation is driven by a change from a tetraloop to a loop E conformation. EMBO J 16:599–610. https://doi.org/10.1093/emboj/16.3.599.
13. Bojic T, Beeharry Y, Zhang DJ, Pelchat M. 2012. Tomato RNA polymerase II interacts with the rod-like conformation of the left terminal domain of the potato spindle tuber viroid positive RNA genome. J Gen Virol 93:1591–1600. https://doi.org/10.1099/vir.0.041574-0.
14. Ding B. 2010. Viroids: self-replicating, mobile, and fast-evolving noncoding regulatory RNAs. Wiley Interdiscip Rev RNA 1:362–375. https://doi.org/10.1002/wrna.22.
15. Flores R, Hernandez C, Martinez de Alba AE, Daros JA, Di Serio F. 2005. Viroids and viroid-host interactions. Annu Rev Phytopathol 43:117–139. https://doi.org/10.1146/annurev.phyto.43.040204.140243.
16. Muhlbach HP, Sanger HL. 1979. Viroid replication is inhibited by alpha-amanitin. Nature 278:185–188. https://doi.org/10.1038/278185a0.
17. Schindler IM, Mühlbach HP. 1992. Involvement of nuclear DNA-dependent RNA polymerases in potato spindle tuber viroid replication: a reevaluation. Plant Science 84:221–229. https://doi.org/10.1016/0168-9452(92)90138-C.
18. Rackwitz HR, Rohde W, Sanger HL. 1981. DNA-dependent RNA polymerase II of plant origin transcribes viroid RNA into full-length copies. Nature 291:297–301. https://doi.org/10.1038/291297a0.
19. Wang Y, Qu J, Ji S, Wallace AJ, Wu J, Li Y, Gopalan V, Ding B. 2016. A land plant-specific transcription factor directly enhances transcription of a pathogenic noncoding RNA template by DNA-dependent RNA polymerase II. Plant Cell 28:1094–1107. https://doi.org/10.1105/tpc.16.00100.
20. Hammond MC, Wachter A, Breaker RR. 2009. A plant 5S ribosomal RNA mimic regulates alternative splicing of transcription factor IIIA pre-mRNAs. Nat Struct Mol Biol 16:541–549. https://doi.org/10.1038/nsmb.1588.
21. Eiras M, Nohales MA, Kitajima EW, Flores R, Daros JA. 2011. Ribosomal protein L5 and transcription factor IIIA from *Arabidopsis thaliana* bind in vitro specifically Potato spindle tuber viroid RNA. Arch Virol 156:529–533. https://doi.org/10.1007/s00705-010-0867-x.
22. Mathieu O, Yukawa Y, Prieto JL, Vaillant I, Sugiura M, Tourmente S. 2003. Identification and characterization of transcription factor IIIA and ribosomal protein L5 from *Arabidopsis thaliana*. Nucleic Acids Res 31:2424–2433. https://doi.org/10.1093/nar/gkg335.
23. Ciganda M, Williams N. 2011. Eukaryotic 5S rRNA biogenesis. Wiley Interdiscip Rev RNA 2:523–533. https://doi.org/10.1002/wrna.74.
24. Zheng Y, Wang Y, Ding B, Fei Z. 2017. Comprehensive transcriptome analyses reveal that potato spindle tuber viroid triggers genome-wide changes inalternative splicing, inducible *trans*-acting activity of phased secondary small interfering RNAs, and immune responses. J Virol 91:e00247-17. https://doi.org/10.1128/JVI.01094-17.
25. Qi Y, Ding B. 2002. Replication of potato spindle tuber viroid in cultured cells of tobacco and *Nicotiana benthamiana*: the role of specific nucleotides in determining replication levels for host adaptation. Virology 302:445–456. https://doi.org/10.1006/viro.2002.1662.
26. Flores R, Di Serio F, Hernández C. 1997. Viroids: the noncoding genomes. Semin Virol 8:65–73. https://doi.org/10.1006/smvy.1997.0107.
27. Fu Y, Bannach O, Chen H, Teune JH, Schmitz A, Steger G, Xiong L, Barbazuk WB. 2009. Alternative splicing of anciently exonized 5S rRNA regulates plant transcription factor TFIIIA. Genome Res 19:913–921. https://doi.org/10.1101/gr.086876.108.
28. Wassenegger M, Spieker RL, Thalmeir S, Gast FU, Riedel L, Sanger HL. 1996. A single nucleotide substitution converts potato spindle tuber viroid (PSTVd) from a noninfectious to an infectious RNA for *Nicotiana tabacum*. Virology 226:191–197. https://doi.org/10.1006/viro.1996.0646.
29. Zhu Y, Qi Y, Xun Y, Owens R, Ding B. 2002. Movement of potato spindle tuber viroid reveals regulatory points of phloem-mediated RNA traffic. Plant Physiol 130:138–146. https://doi.org/10.1104/pp.006403.
30. Qi Y, Ding B. 2003. Inhibition of cell growth and shoot development by a specific nucleotide sequence in a noncoding viroid RNA. Plant Cell 15:1360–1374. https://doi.org/10.1105/tpc.011585.
31. Itaya A, Matsuda Y, Gonzales RA, Nelson RS, Ding B. 2002. Potato spindle tuber viroid strains of different pathogenicity induces and suppresses expression of common and unique genes in infected tomato. Mol Plant Microbe Interact 15:990–999. https://doi.org/10.1094/MPMI.2002.15.10.990.
32. Owens RA, Tech KB, Shao JY, Sano T, Baker CJ. 2012. Global analysis of tomato gene expression during potato spindle tuber viroid infection reveals a complex array of changes affecting hormone signaling. Mol Plant Microbe Interact 25:582–598. https://doi.org/10.1094/MPMI-09-11-0258.
33. Zheng Y, Ding B, Fei Z, Wang Y. 2017. Comprehensive transcriptome analyses reveal tomato plant responses to tobacco rattle virus-based gene silencing vectors. Sci Rep 7:9771. https://doi.org/10.1038/s41598-017-10143-1.
34. Mandadi KK, Scholthof KB. 2015. Genome-wide analysis of alternative splicing landscapes modulated during plant-virus interactions in *Brachypodium distachyon*. Plant Cell 27:71–85. https://doi.org/10.1105/tpc.114.133991.
35. Huang J, Gu L, Zhang Y, Yan T, Kong G, Kong L, Guo B, Qiu M, Wang Y, Jing M, Xing W, Ye W, Wu Z, Zhang Z, Zheng X, Gijzen M, Wang Y, Dong S. 2017. An oomycete plant pathogen reprograms host pre-mRNA splicing to subvert immunity. Nat Commun 8:2051. https://doi.org/10.1038/s41467-017-02233-5.
36. Pan H, Oztas O, Zhang X, Wu X, Stonoha C, Wang E, Wang B, Wang D. 2016. A symbiotic SNARE protein generated by alternative termination of transcription. Nat Plants 2:15197. https://doi.org/10.1038/nplants.2015.197.
37. Dinesh-Kumar SP, Baker BJ. 2000. Alternatively spliced N resistance gene transcripts: their possible role in tobacco mosaic virus resistance. Proc Natl Acad Sci U S A 97:1908–1913. https://doi.org/10.1073/pnas.020367497.
38. Bardou F, Ariel F, Simpson CG, Romero-Barrios N, Laporte P, Balzergue S, Brown JW, Crespi M. 2014. Long noncoding RNA modulates alternative splicing regulators in *Arabidopsis*. Dev Cell 30:166–176. https://doi.org/10.1016/j.devcel.2014.06.017.
39. Flores R, Navarro B, Kovalskaya N, Hammond RW, Di Serio F. 2017. Engineering resistance against viroids. Curr Opin Virol 26:1–7. https://doi.org/10.1016/j.coviro.2017.07.003.
40. Dalakouras A, Dadami E, Wassenegger M. 2015. Engineering viroid resistance. Viruses 7:634–646. https://doi.org/10.3390/v7020634.
41. Sano T, Nagayama A, Ogawa T, Ishida I, Okada Y. 1997. Transgenic potato expressing a double-stranded RNA-specific ribonuclease is resistant to potato spindle tuber viroid. Nat Biotechnol 15:1290–1294. https://doi.org/10.1038/nbt1197-1290.
42. Bolger AM, Lohse M, Usadel B. 2014. Trimmomatic: a flexible trimmer for Illumina sequence data. Bioinformatics 30:2114–2120. https://doi.org/10.1093/bioinformatics/btu170.
43. Bombarely A, Rosli HG, Vrebalov J, Moffett P, Mueller LA, Martin GB. 2012. A draft genome sequence of *Nicotiana benthamiana* to enhance molecular plant-microbe biology research. Mol Plant Microbe Interact 25:1523–1530. https://doi.org/10.1094/MPMI-06-12-0148-TA.
44. Langmead B, Trapnell C, Pop M, Salzberg SL. 2009. Ultrafast and memory-efficient alignment of short DNA sequences to the human genome. Genome Biol 10:R25. https://doi.org/10.1186/gb-2009-10-3-r25.